JOURNAL OF AIRCRAFT
Vol. 46, No. 2, March–April 2009

Ideal Lift Distributions and Flap Angles for Adaptive Wings

Ashok Gopalarathnam* and Rachel King Norris†
North Carolina State University, Raleigh, North Carolina 27695-7910

DOI: 10.2514/1.38713

An approach is presented for determining the optimum flap angles and spanwise loading to suit a given flight condition. Multiple trailing-edge flaps along the span of an adaptive wing are set to either reduce drag in rectilinear flight conditions or to limit the wing bending moment at maneuvering conditions. For reducing drag, the flaps are adjusted to minimize induced drag, while simultaneously enabling the wing sections to operate within their respective low-drag ranges. For limiting wing bending moment, the flaps are used to relieve the loading near the wing tips. An important element of the approach is the decomposition of the flap angles into a distribution that can be used to control the spanwise loading for induced-drag control and a constant flap that can used for profile-drag control. The problem is linearized using the concept of basic and additional lift distributions, which enables the use of standard constrained-minimization formulations. The results for flap-angle distributions for different flight conditions are presented for a planar and a nonplanar wing. Postdesign analysis and aircraft-performance simulations are used to validate the optimum flap-angle distributions determined using the current approach.

Nomenclature

B	=	wing root bending moment
b	=	wing span
C_B	=	wing root bending moment coefficient
C_D	=	aircraft or wing drag coefficient
C_d	=	airfoil or section drag coefficient
C_L	=	aircraft or wing lift coefficient
C_l	=	airfoil or section lift coefficient
c	=	local chord
D	=	wing drag
$\mathbf{D}$	=	matrix of drag coefficients
$f(\boldsymbol{x})$	=	objective function of multiple variables $\boldsymbol{x}$
$g(\boldsymbol{x})$	=	constraint function of multiple variables $\boldsymbol{x}$
H	=	modified objective function
L'	=	spanwise lift distribution
S	=	wing planform area
u	=	component of induced velocity in the freestream direction
V_∞	=	freestream velocity
W	=	weighting factor
w	=	spanwise distribution of Trefftz plane downwash
x_f	=	chordwise location of flap hinge
y	=	spanwise coordinate
α	=	angle of attack
Γ	=	spanwise distribution of bound-vorticity strength
$\boldsymbol{\delta_f}$	=	flap-angle distribution
δ_f	=	flap angle
$\boldsymbol{\delta}_{\text{mean}}$	=	elemental mean flap-angle distribution
$\boldsymbol{\delta}_{\boldsymbol{f}}$	=	variation flap-angle distribution
δ_f	=	mean flap angle
θ_f	=	angular coordinate of flap hinge
Λ	=	local dihedral angle
λ	=	Lagrange multiplier
ρ	=	density of air

Subscripts

a	=	additional
$a, 1$	=	additional distribution at $C_L = 1$
b	=	basic
i, j	=	flap indices
ind	=	induced
low	=	lower corner of low-drag range with most-negative flap angle
max	=	maximum, most-positive flap angle
min	=	minimum, most-negative flap angle
N	=	number of trailing-edge flaps on the wing
ref	=	reference
up	=	upper corner of low-drag range with most-positive flap angle
0	=	zero-flap condition
$0l$	=	zero lift

Presented as Paper 4722 at the 22nd Applied Aerodynamics Conference and Exhibit, Providence, Rhode Island, 16–19 August 2004; received 23 May 2008; revision received 17 September 2008; accepted for publication 19 September 2008.

*Associate Professor, Box 7910; ashok_g@ncsu.edu. Senior Member AIAA.

†Graduate Research Assistant; currently Aerospace Engineer, ManTech SRS—Washington Group. Member AIAA.

I. Introduction

IT IS believed that birds take advantage of their variable-geometry wings to achieve near-optimum spanwise lift distributions for various flight conditions. In contrast, most current-day aircraft with rigid wings have less flexibility to adapt their wing geometry, except for the use of high-lift devices. Over the past decade, there has been renewed interest [1–7] in the use of adaptive or morphing lifting surfaces in an effort to optimize an aircraft for several flight conditions. Wing-shape adaptation via spanwise camber variation can be used not only to reduce profile and induced drag, but also to reduce wing weight with structural-load alleviation at maneuvering conditions by redistributing the spanwise load distribution [1,5,6]. Overall, these benefits can lead to reduced fuel burn and lower emissions.

Spanwise camber change can be accomplished by a variety of means, but one mechanism of shape adaptation attracting considerable interest is the use of multiple trailing-edge (TE) flaps along the wingspan, as shown in Fig. 1. For several years now, high-performance sailplanes have been using the benefits of multiple TE flaperons for drag reduction and roll control. In 1992, Spillman [1] provided general guidelines for the sizing and scheduling of multiple TE flaps. He pointed out that the possible reductions in drag and wing weight could result in significant reductions in fuel usage and operating costs, in comparison to a fixed-geometry wing designed for the same application.

In the United States, aircraft-performance benefits from the use of multiple TE flaps were estimated in 1999 by Bolonkin and Gilyard [4] to be as much as 10% at nonstandard conditions and 3% at cruise conditions. Bolonkin and Gilyard suggested that such

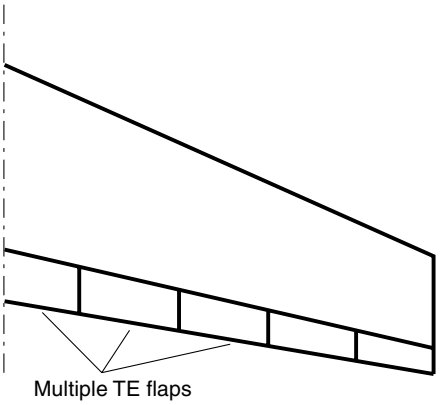

Fig. 1 Multiple TE flaps on a swept wing.

benefits could result in a savings of as much as $300,000 per year for a transport aircraft in fuel costs alone. With the current trend toward fuel costs becoming an increasing proportion of the operating costs, such savings are worth pursuing. An example of an in-flight application of spanwise variable camber is the maneuver load control flight experiment of the AFTI/F-111 advanced-fighter aircraft [2] at the NASA Dryden Flight Research Center. In this experiment, the spanwise camber flap positions were commanded as a function of true airspeed, Mach number, dynamic pressure, normal acceleration, and sweep position (of the variable-sweep wing). The measured loads indicated that the load factor can increase as much as 1.0 g without any increase in the root-bending moment by a redistribution of the spanwise lift toward the wing root [2]. More recent efforts [5–9] indicate the continuing interest in adaptive-wing technology.

Motivated by the continued interest in the use of TE flaps for spanwise camber change and the estimated benefits from adaptive-wing technology, the aim of the current work was to develop a generalized approach to determine the ideal lift distributions and flap angles for an adaptive wing at various flight conditions. The approach builds on the superposition of basic and additional lift distributions, which results in a simple and elegant solution procedure. The approach also provides insight into the simultaneous reduction of induced and profile drag along with the ability to handle structural constraints. The objective was to develop a method for use not only in wing design, but one that could also provide inputs for the optimal scheduling of flaps for different flight conditions. The profile-drag reduction portion of the current work is applicable to natural-laminar-flow (NLF) wings, but can be extended to other wings as well.

In the following sections, background information relevant to the development of the approach is presented, followed by the methodology that determines the optimum flap angles for minimum drag with or without a wing root bending moment (RBM) constraint. The optimum lift distributions and flap angles at multiple operating conditions are then presented for two example wings. Postdesign analysis and aircraft-performance simulations are used to validate the optimum flap-angle distributions determined by the current approach and to determine the resulting improvements to aircraft performance.

II. Background

This section includes background information on the elements of applied aerodynamics and mathematics relevant to the development of the current method. The background is presented in four subsections. Section II.A describes the theory of basic and additional lift distributions. Section II.B presents equations for the induced drag of superposed lift distributions. Section II.C briefly reviews equations for the relative extrema of multivariable functions with constraints. And Sec. II.D briefly reviews the use of a TE flap for drag-bucket control on an airfoil section.

A. Basic and Additional Lift Distributions

The concept of basic and additional lift distributions is described in several references [10–12]. The use of this concept enables the determination of flap angles using a simple, semi-analytical approach. In this subsection, this concept is briefly reviewed.

Within the assumption of linear aerodynamics (a linear C_l-α variation and a linear C_l-Γ relationship), the spanwise distribution of bound circulation (or, alternatively, lift distribution) over a wing can be expressed as a sum of two contributions: 1) basic distribution, $\Gamma_b(y)$; and 2) additional distribution, $\Gamma_a(y)$:

$$\Gamma(y) = \Gamma_b(y) + \Gamma_a(y) \tag{1}$$

The basic distribution, Γ_b, is the Γ distribution at $C_L = 0$ and is the result of spanwise variations in geometric twist, aerodynamic twist due to camber, and flap deflections. Furthermore, the Γ_b distributions due to twist, camber, or flap deflection scale linearly with that particular parameter, and individual Γ_b distributions can be added to obtain the total Γ_b distribution. For example, the total Γ_b due to wing twist, spanwise camber variation, and flap-angle variation is simply the sum of the individual Γ_b distributions:

$$\Gamma_b(y) = \Gamma_{b,\text{twist}}(y) + \Gamma_{b,\text{camber}}(y) + \Gamma_{b,\text{flap}}(y) \tag{2}$$

The additional Γ distribution, Γ_a, is due to changes to α for the wing with zero geometric and aerodynamic twist. It is, therefore, independent of geometric and aerodynamic twist and scales with the wing C_L. Thus, the additional Γ distribution for $C_L = 1$, written as $\Gamma_{a,1}$, can be precomputed for a wing and used to compute the Γ_a for any C_L, as follows:

$$\Gamma_a(y) = C_L \Gamma_{a,1}(y) \tag{3}$$

If the component of the induced velocities along the freestream direction, u, are assumed to be small compared with V_∞, then the magnitude of the local loading is proportional to the local Γ distribution:

$$L'(y) = \rho(V_\infty + u(y))\Gamma(y) \approx \rho V_\infty \Gamma(y) \tag{4}$$

which results in the following linear relationship between Γ and the local lift coefficient, C_l:

$$C_l(y) = \frac{2\Gamma(y)}{c(y)V_\infty} \tag{5}$$

It is, therefore, possible to write the spanwise C_l distribution using superposition as follows:

$$C_l(y) = C_{lb,\text{twist}}(y) + C_{lb,\text{camber}}(y) + C_{lb,\text{flap}}(y) + C_L C_{la,1}(y) \tag{6}$$

B. Induced Drag of Superposed Lift Distributions

It is well known that, for a given bound-circulation distribution, the induced drag, D_{ind}, can be obtained by integration along the wake trace in the Trefftz plane (see [13] or [14]) as follows:

$$D_{\text{ind}} = \frac{\rho}{2}\int_{-\frac{b}{2}}^{\frac{b}{2}} \Gamma(y) w(y)\, \mathrm{d}y \tag{7}$$

where $w(y)$ is the Trefftz-plane downwash distribution. This equation has been written for a planar wing with a rigid wake spanning from $y = -(b/2)$ to $y = (b/2)$. However, it can be readily extended to a nonplanar wing by integrating along the arc length of the wake trace and using the component of the induced velocity normal to the wake trace instead of the downwash.

In nondimensional form, the induced-drag coefficient, $C_{D\text{ind}}$, can be written as:

$$C_{D\text{ind}} = \frac{1}{2S_{\text{ref}}}\int_{-\frac{b}{2}}^{\frac{b}{2}} c(y) C_l(y) \frac{w(y)}{V_\infty}\, \mathrm{d}y \tag{8}$$

where $w(y)/V_\infty$ is the spanwise distribution of the downwash angle in the Trefftz plane.

Noting that the $w(y)$ distributions can also be constructed using superposition of basic and additional distributions, similar to the $C_l(y)$ distribution in Eq. (6), the total induced-drag coefficient can be written using superposition. As an illustration, consider a superposed lift distribution constructed from two distributions, P and Q. The total induced-drag coefficient of the superposed lift distribution can be written as

$$C_{D\text{ind}} = C_{DPP} + C_{DPQ} + C_{DQP} + C_{DQQ} \tag{9}$$

where, for each term on the right-hand side, the first subscript indicates the source of the $c(y)C_l(y)$ distribution and the second subscript indicates the source of the $w(y)/V_\infty$ distribution. For example,

$$C_{DPQ} = \frac{1}{2S_{\text{ref}}} \int_{-\frac{b}{2}}^{\frac{b}{2}} c(y) C_{lP}(y) \frac{w_Q(y)}{V_\infty} \, \mathrm{d}y \tag{10}$$

Furthermore, using Munk's mutual-drag theorem [15], the expression for the total induced-drag coefficient can be further simplified because $C_{DPQ} = C_{DQP}$ and so on.

C. Relative Minima of Multivariable Functions with Constraints

Consider a function of several variables, $f(\boldsymbol{x})$, which has first and second partial derivatives everywhere. The necessary condition [16] for a minimum in f is that the first derivative with respect to all the variables, $\boldsymbol{x}$, should be zero, as follows:

$$\partial f / \partial \boldsymbol{x} = 0 \tag{11}$$

The sufficient condition for a minimum is that the Hessian matrix composed of the terms $\partial^2 f / \partial x_i \partial x_j$, evaluated at the extremum from Eq. (11), be positive definite.

With the addition of an equality constraint, $g(\boldsymbol{x}) = 0$, the constrained minimum of $f(\boldsymbol{x})$ can be determined by using a Lagrange multiplier, λ. The new objective function, to be minimized, is now written as $H(\boldsymbol{x}, \lambda) = f(\boldsymbol{x}) + \lambda g(\boldsymbol{x})$. The necessary condition for the constrained minimum is that the first derivative of H with respect to all $\boldsymbol{x}$ and λ should be zero, as follows:

$$\partial H / \partial \boldsymbol{x} = 0, \qquad \partial H / \partial \lambda = 0 \tag{12}$$

and the sufficient condition is that the corresponding Hessian matrix be positive definite.

D. Trailing-Edge Flap for Drag-Bucket Control

For flight at low subsonic Mach numbers, the wing profile drag is dominated by the skin-friction drag when there is no separated flow and associated pressure drag. To minimize profile drag, airfoils are often designed to have significant regions of favorable pressure gradient on both the upper and lower surfaces to support laminar flow. Such NLF airfoils typically have a distinct low-drag range, or drag bucket, which is the range of lift coefficients over which low drag is achieved. To extend the range of lift coefficients over which low drag is achieved, a trailing-edge "cruise" flap is often used. First introduced by Pfenninger [17,18], it has since been used on several airfoil designs [19–23], especially airfoils for high-performance sailplanes [21].

Figure 2 illustrates the effect of a trailing-edge flap on the low-drag range of the NASA NLF(1)-0215F airfoil [19], which is used as an example. It is seen that a positive (TE down) flap-angle results in the low-drag range moving to higher values of C_l and vice versa for a negative flap angle. Thus, it is seen that a low-profile C_d is achieved over a larger C_l range using a TE flap than without the flap. This benefit is limited to a small range of flap angles, typically close to ± 10 deg, beyond which flow separation near the flap hinge results in large pressure drag, which negates the benefit from the reduction in skin-friction drag. These limiting values of flap angle, when the flap is used for drag reduction, are referred to in this paper as the most-negative flap angle, $\delta_{f_{\min}}$, and the most-positive flap angle, $\delta_{f_{\max}}$. Using the results for the NLF(1)-0215F airfoil in Fig. 2 as an example, low C_d can be achieved over a C_l ranging from a $C_{l\text{low}}$ of 0.2, achieved with the $\delta_{f_{\min}}$ of a -10 deg flap, to a $C_{l\text{up}}$ of 1.3, achieved with the $\delta_{f_{\max}}$ of a $+10$ deg flap. For any value of operating C_l that lies between $C_{l\text{low}}$ and $C_{l\text{up}}$, using a flap angle that is determined by linear interpolation between $\delta_{f_{\min}}$ and $\delta_{f_{\max}}$ will result in a smooth variation of the TE flap angle with operating C_l, while ensuring low C_d.

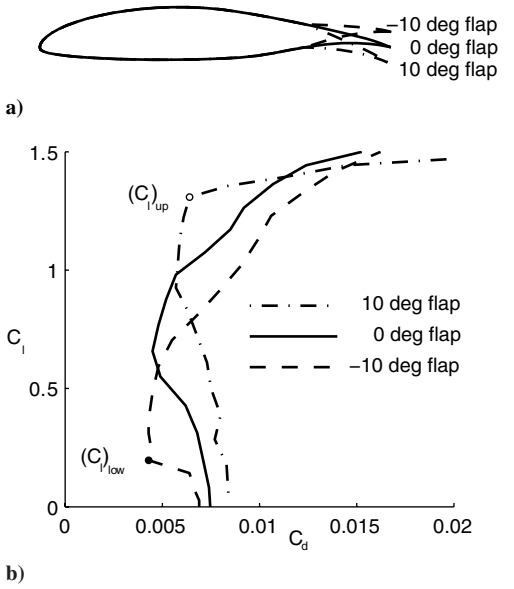

Fig. 2 Effect of TE flap angle on the drag polar for the NASA NLF(1)-0215 airfoil: a) geometry, and b) drag polars from wind-tunnel experiments [19] at a Reynolds number of 6×10^6.

III. Methodology

The aim of the methodology is to determine the optimum TE flap angles that will minimize profile and induced drag, while satisfying any constraints on the wing bending moment resulting from the spanwise loading. This problem, at first, appears to be quite nonlinear, because changing any flap angle will affect the loading on the entire wing, thus changing the operating C_L and the section C_l over the portions of the wing controlled by the other flaps. Such a problem can be solved using a nonlinear optimizer that uses a wing analysis routine as a function evaluation. In the current approach, however, a different strategy has been used to linearize the problem and simplify the solution procedure, while providing insight for design. For this linearization, the desired lift distribution is described in terms of the unknown flap angles using the superposition of basic and additional loading. Further, profile- and induced-drag dependencies on the flap angles have been decoupled by decomposing the flap angles into a mean flap and a variation flap-angle distribution. The details of this methodology are described in the following subsections.

A. Superposition of Lift Distributions

The advantage of using the superposition concept is that the net C_l distribution for a particular wing C_L can be posed in terms of the unknown flap angles. Assuming N flaps on the wing, the expression for the net C_l distribution is

$$C_l = C_L C_{la,1} + C_{lb,0} + C_{lb,1}\delta_{f,1} + C_{lb,2}\delta_{f,2} + \cdots + C_{lb,N}\delta_{f,N} \tag{13}$$

where $C_{lb,0}$ is the zero-flap basic C_l distribution due to the geometric and aerodynamic twist resulting from spanwise changes to the wing airfoil. The increment in basic C_l distribution due to a unit flap deflection for flap i is denoted by $C_{lb,i}$.

The total induced-drag coefficient, $C_{D\text{ind}}$, can be expressed using all combinations of pairs formed by the different elementary lift distributions as follows:

$$C_{D\text{ind}} = C_{Daa}C_L^2 + C_{D00} + (C_{Da0} + C_{D0a})C_L + \sum_{j=1}^{N}(C_{Daj}C_L + C_{Dja}C_L + C_{D0j} + C_{Dj0})\delta_{f,j} + \sum_{i=1}^{N}\sum_{j=1}^{N} C_{Dij}\delta_{f,i}\delta_{f,j} \tag{14}$$

which can be written compactly in matrix notation as

$$C_{D\text{ind}} = \mathbf{f}^T\mathbf{D}\mathbf{f} \tag{15}$$

where $\mathbf{f}^T$, the transpose of $\mathbf{f}$, is written as

$$\mathbf{f}^T = \begin{bmatrix} C_L & 1 & \delta_{f,1} & \dots & \delta_{f,N} \end{bmatrix} \tag{16}$$

and the drag-coefficient matrix, $\mathbf{D}$, is written as

$$\mathbf{D} = \begin{bmatrix} C_{Daa} & C_{Da0} & C_{Da1} & \dots & C_{DaN} \\ C_{D0a} & C_{D00} & C_{D01} & \dots & C_{D0N} \\ C_{D1a} & C_{D10} & C_{D11} & \dots & C_{D1N} \\ \vdots & \vdots & \vdots & & \vdots \\ C_{DNa} & C_{DN0} & C_{DN1} & \dots & C_{DNN} \end{bmatrix} \tag{17}$$

in which the elements of the $\mathbf{D}$ matrix are defined in a manner similar to Eq. (10). As an illustration, C_{Da0} is written as

$$C_{Da0} = \frac{1}{2S_{\text{ref}}}\int_{-\frac{b}{2}}^{\frac{b}{2}} c(y)C_{la,1}(y)\frac{w_{b,0}(y)}{V_\infty}\,\mathrm{d}y \tag{18}$$

The elements of the $\mathbf{D}$ matrix can be computed using any wing analysis method, such as a panel, vortex lattice, Weissinger-type, or lifting-line method, that outputs the spanwise C_l and w/V_∞ distributions at a specified C_L. For computing the $\mathbf{D}$ matrix, such an analysis method is used to analyze $N+2$ cases: the additional-loading case, the zero-flap basic loading case, and the N basic-loading cases for the N flaps. Owing to Munk's mutual-drag theorem [15], the $\mathbf{D}$ matrix should be symmetric. If the $\mathbf{D}$ matrix has slight asymmetry due to nonlinearities or numerical errors in the analysis method, then it can be made symmetric by averaging it with its transpose.

For an illustration of the concept, an example wing with a vertical winglet of height $0.125b/2$ is considered. This wing was analyzed using the AVL (Athena Vortex Lattice) code [24]. Four TE flaps are located along the span of the planar portion of the wing and one on the winglet, with each flap on the planar portion having the same span and flap-to-chord ratio of 0.2. In this particular example, the wing is assumed to have zero geometric twist and zero section camber. In Fig. 3a, the $C_{la,1}$ for the wing, computed using AVL, is shown. Also shown are the C_{lb} distributions (scaled by 10 times, for clarity) from AVL for 1 deg deflections of 1) flap 3, and 2) flap 5, located on the winglet. Only the right side of the wing is shown because of symmetry.

C_l distribution for this wing at $C_L = 0.5$ with flap 3 deflected to $\delta_f = 5$ deg and flap 5 deflected to $\delta_f = -10$ deg was then computed using the AVL code. This distribution from direct analysis is compared in Fig. 3b with the distribution achieved by superposition of 1) $C_{la,1}$ scaled by 0.5, 2) C_{lb} for flap 3 scaled by 5, and 3) C_{lb} for flap 5 scaled by -10. The $C_{D\text{ind}}$ for this configuration from AVL is 0.00838 and from superposition is 0.00842 [Eq. (14)]. The excellent comparison of the C_l distribution and the $C_{D\text{ind}}$ value illustrates the effectiveness of the superposition of lift distributions, even when there are large gradients in the spanwise loading and associated strong trailing vortices at the flap tips.

B. Minimization of the Induced Drag

A necessary condition for minimum induced drag is that the first derivatives of the $C_{D\text{ind}}$ with respect to all the flap angles should be zero. As an illustration, the derivative with respect to flap j is set equal to zero as follows:

$$\frac{\partial C_{D\text{ind}}}{\partial \delta_{f,j}} = (C_{Daj} + C_{Dja})C_L + (C_{D0j} + C_{Dj0}) + \sum_{i=1}^{N}(C_{Dij} + C_{Dji})\delta_{f,i} = 0 \tag{19}$$

The resulting system of N equations can be expressed in compact form as

$$\begin{bmatrix} C_{D11} & \dots & C_{D1N} \\ \vdots & & \vdots \\ C_{DN1} & \dots & C_{DNN} \end{bmatrix} \begin{Bmatrix} \delta_{f,1} \\ \vdots \\ \delta_{f,N} \end{Bmatrix} = -\begin{Bmatrix} C_L C_{Da1} + C_{D01} \\ \vdots \\ C_L C_{DaN} + C_{D0N} \end{Bmatrix} \tag{20}$$

in which Munk's mutual-drag theorem has been used to simplify the vector on the right-hand side.

In many cases, when the multiple flaps occupy the entire span of the wing, the square matrix on the left-hand side of Eq. (20) is singular and has a rank $(N-1)$ for a wing with N flaps. In other words, the N equations are not linearly independent. The reason for this behavior is explained by considering a planar wing with all flaps having the same flap-to-chord ratio. For this wing, it is noted that a uniform deflection of all the flaps by the same angle will not change the basic loading, but will only change the additional loading if the

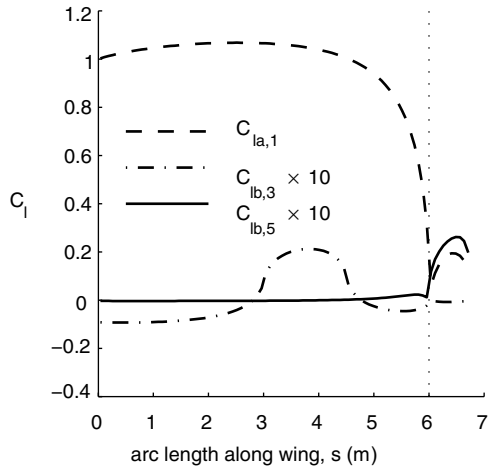

a)

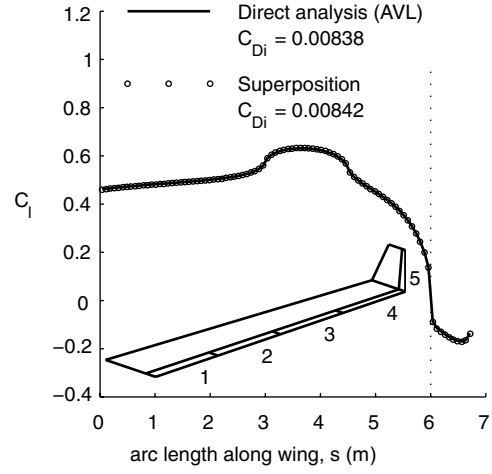

b)

Fig. 3 Illustration of superposition: a) basic and additional C_l distributions, and b) C_l due to superposition compared with C_l from direct analysis. Inset shows right side of geometry.

wing angle of attack is held constant. Similarly, it is noted that, for this wing, the *basic loading* due to a 1 deg deflection of flap j can be replicated exactly by instead deflecting all the other flaps to -1 deg, because any combination of basic loadings will integrate to zero wing C_L. It follows that the numbers in any row of the square matrix in Eq. (20) can be computed by taking the negative of the sum of the numbers in all the other rows. Considering an element of the Nth row as an example, we see that C_{DNj} can be written as the negative of the sum of all the other elements of the jth column, as follows:

$$\begin{aligned} C_{DNj} &= \frac{1}{2S_{\text{ref}}} \int_{-\frac{b}{2}}^{\frac{b}{2}} c(y) C_{lb,N}(y) \frac{w_{b,j}(y)}{V_\infty} \, \mathrm{d}y \\ &= \frac{1}{2S_{\text{ref}}} \int_{-\frac{b}{2}}^{\frac{b}{2}} c(y) \left(-\sum_{k=1}^{N-1} C_{lb,k}(y) \right) \frac{w_{b,j}(y)}{V_\infty} \, \mathrm{d}y \\ &= -\sum_{k=1}^{N-1} C_{Dkj} \end{aligned} \tag{21}$$

This lack of linear independence of the square matrix poses a problem for the solution of Eq. (20), because there are an infinite number of solutions for the optimum flap angles. Consequently, an additional equation is needed to solve the system.

C. Decomposition of the Flap-Angle Distribution

A solution to this problem of the linear dependence of the N equations is to decompose the desired optimum flap-angle distribution into 1) a "mean flap-angle distribution" that, in a manner similar to the wing angle of attack, can be used to increase the wing C_L without causing any changes to the basic loading; and 2) a "variation flap-angle distribution" that contributes only to the basic loading and has a weighted mean angle of 0 deg, so as to not contribute to a change in the wing C_L. The major advantages of this decomposition are that the mean flap behaves much like a cruise flap (see Sec. II.D), which can be used to adapt the wing camber for profile-drag reduction via drag-bucket control, and that the variation flap can be used independently to minimize the induced drag (with or without constraints). Another advantage is that, when using the variation flap-angle distribution, the additional equation sought to enable the solution of Eq. (20) is provided by requiring that the weighted mean of the variation flap-angle distribution be equal to zero.

Thus, the desired optimum flap-angle distribution, $\boldsymbol{\delta}_f$, is written as a sum of a mean flap-angle distribution, $\bar{\delta}_f \boldsymbol{\delta}_{\mathbf{mean}}$, and a variation flap-angle distribution, $\hat{\boldsymbol{\delta}}_f$:

$$\boldsymbol{\delta}_f = \bar{\delta}_f \boldsymbol{\delta}_{\mathbf{mean}} + \hat{\boldsymbol{\delta}}_f \tag{22}$$

D. Mean Flap-Angle Distribution

In Eq. (22), the term $\boldsymbol{\delta}_{\mathbf{mean}}$ is the elemental mean flap-angle distribution that does not result in any basic loading on the wing. This flap-angle distribution results in a change in the additional loading on the wing similar to a 1 deg deflection of a full-span flap on the wing with a uniform flap-to-chord ratio along the span. Even when scaled by the value of the mean flap, $\bar{\delta}_f$, the resulting mean flap-angle distribution results only in an additional loading and no basic loading. In this respect, a change to the value of the mean flap is similar to a change in the wing angle of attack.

When the multiple TE flaps on a planar wing all have the same flap-to-chord ratio (or the same value for the x/c of the flap hinge), then the elements of the $\boldsymbol{\delta}_{\mathbf{mean}}$ vector are all equal to 1 and the mean flap results in a uniform deflection of all the TE flaps by $\bar{\delta}_f$. In a more general case, however, when the TE flaps have different flap-to-chord ratios and/or when the local dihedral angle is different on different portions of the wing, then the element of the $\boldsymbol{\delta}_{\mathbf{mean}}$ vector corresponding to a flap gets set by 1) the local flap effectiveness, and 2) the contribution of the loading from that portion of the wing to the wing lift. In such a case, one of the flaps is designated as a "reference flap," and the value of δ_{mean} for this flap is set to 1. The values for δ_{mean} for all the other flaps are determined as follows:

$$\delta_{\text{mean},i} = \frac{\tau_{\text{ref}} \cos(\Lambda_i)}{\tau_i \cos(\Lambda_{\text{ref}})} \tag{23}$$

where τ is the flap effectiveness factor, or the equivalent change in airfoil angle of attack per degree of flap deflection; Λ is the local dihedral angle; and the subscript ref refers to the reference flap. The flap effectiveness factor for plain flaps in inviscid flow is directly dependent on the x_f/c location of the hinge and can be determined from an airfoil analysis method or from thin airfoil theory (see [12]) as

$$\tau = \frac{-\Delta\alpha_{0l}}{\delta_f} = 1 - \frac{\theta_f}{\pi} + \frac{\sin\theta_f}{\pi} \tag{24}$$

in which all angles are in radians and θ_f, the angular coordinate for the hinge location, is related to the x_f/c of the hinge location as follows:

$$\theta_f = \cos^{-1}(1 - 2(x_f/c)) \tag{25}$$

The $\cos(\Lambda)$ terms in Eq. (23) take into consideration that portions of the wing with a large dihedral contribute less to the wing lift, as their loading results in a force that is at least partly oriented in the sideways direction. For illustration, consider a TE flap on a winglet with a 90 deg dihedral angle. This flap will result in some basic loading at any angle other than 0 deg. Thus, the $\cos(\Lambda)$ factor ensures that the TE flap on a 90 deg winglet will be zero for the mean flap-angle distribution.

E. Drag-Bucket Control with the Mean Flap

As explained in Sec. II.D, a TE flap on an NLF airfoil can be used to adjust the drag bucket so that the low-drag range envelopes the operating C_l of the airfoil. Because the mean flap on the wing, $\bar{\delta}_f$, behaves much like a trailing-edge flap on an airfoil, the mean flap is set appropriately for the wing C_L to ensure that a majority of the wing sections are operating within the low-drag ranges of their respective sections. This is achieved by linear interpolation between $(C_{l\text{low}}, \delta_{f_{\min}})$ and $(C_{l\text{up}}, \delta_{f_{\max}})$ for the operating C_L, as follows:

$$\bar{\delta}_f = \delta_{f_{\min}} + \frac{C_L - C_{l\text{low}}}{C_{L\text{up}} - C_{l\text{low}}} (\delta_{f_{\max}} - \delta_{f_{\min}}) \tag{26}$$

Although this linear variation of $\bar{\delta}_f$ with C_L works well for wings with NLF airfoils with well-defined drag buckets, other variations may be desirable for airfoils such as those used on low-Reynolds-number aircraft. Regardless of the specific type of $\bar{\delta}_f$–C_L variation used, the generality of the current approach is not affected, because the mean and variation flaps independently control the profile- and induced-drag components, respectively.

F. Variation Flap-Angle Distribution

The requirement that, by definition, the variation flap-angle distribution not contribute to the wing C_L leads to the equation that sets the weighted mean of the variation flap angles to zero, as follows:

$$W_1 \hat{\delta}_{f,1} + \cdots + W_N \hat{\delta}_{f,N} = 0 \tag{27}$$

where the weighting factor for each flap takes into consideration the relative influence of that flap on the lift of the wing. For a planar wing, the weighting factor for a given flap may be determined by simply taking the ratio of the area of the wing affected by the flap to the total wing area. An alternate and more rigorous approach that is also applicable to nonplanar geometries can be developed, especially when using an analysis method for determining the elements of the $\mathbf{D}$ matrix. In this approach, the weighting factor for a given flap is the ratio of the angle of attack for the basic loading with a unit deflection of this flap to the sum of the basic-loading angles of attack for all the flaps, as follows:

$$W_j = \frac{\alpha_{b,j}}{\alpha_{b,1} + \cdots + \alpha_{b,N}} \tag{28}$$

where $\alpha_{b,j}$ is the angle of attack for basic loading with a 1 deg angle of flap j. These angles of attack can be determined as part of the same analyses used in the computation of the elements of the **D** matrix without the need for any additional analyses. With the addition of this equation to Eq. (20), the system of equations for the solution of the variation flap angles for the minimization of induced drag becomes

$$\begin{bmatrix} C_{D11} & \cdots & C_{D1N} \\ \vdots & & \vdots \\ C_{DN1} & \cdots & C_{DNN} \\ W_1 & \cdots & W_N \end{bmatrix} \begin{Bmatrix} \hat{\delta}_{f,1} \\ \vdots \\ \hat{\delta}_{f,N} \end{Bmatrix} = -\begin{Bmatrix} C_L C_{Da1} + C_{D01} \\ \vdots \\ C_L C_{DaN} + C_{D0N} \\ 0 \end{Bmatrix} \tag{29}$$

As seen, Eq. (29) has $N + 1$ equations but only N unknowns. This system can be solved either by eliminating any one of the first N equations or by solving the overdetermined system using a least-squares approach. Note also that the variation flap angles have been used in Eq. (29), because the mean flap angle does not affect the basic loading and, hence, does not affect the $C_{D\text{ind}}$.

G. Bending Moment Constraint

One of the advantages of multiple TE flaps is that they can be deflected to provide bending moment relief during maneuvering conditions. The current methodology can be used to determine the variation flap-angle distribution that will result in minimum induced drag with a constraint on the bending moment at a specified spanwise location on the wing. As an illustration, this paper considers the imposition of a bending moment constraint at the wing root.

For convenience, the root bending moment, B, is written in nondimensional form as the root bending moment coefficient, C_B. C_B can be written using superposition of elementary solutions as follows:

$$C_B = \frac{B}{\frac{1}{2}\rho V_\infty^2 S_{\text{ref}} b_{\text{ref}}} = C_L C_{Ba,1} + C_{Bb,0} + C_{Bb,1}\hat{\delta}_{f,1} + \cdots + C_{Bb,N}\hat{\delta}_{f,N} \tag{30}$$

where $C_{Ba,1}$ is the C_B due to the additional loading at $C_L = 1$, $C_{Bb,0}$ is the C_B due to the zero-flap basic loading, and $C_{Bb,j}$ is the C_B due to the incremental basic loading resulting from a 1 deg deflection of flap j. In Eq. (30), the variation flap angles have been used because the mean flap angle does not affect the basic loading. Each of these elementary C_B values can be readily precomputed from the known basic and additional loadings. For example, $C_{Bb,j}$ is determined as follows:

$$C_{Bb,j} = \frac{1}{S_{\text{ref}} b_{\text{ref}}} \int_0^{\frac{b}{2}} c(y) C_{lb,j}(y) y \, \mathrm{d}y \tag{31}$$

If the root bending moment is constrained to a desired value of $C_{B\text{desired}}$, then the new objective function is written by adjoining the constraint equation as follows:

$$H(\hat{\boldsymbol{\delta}}_f, \lambda) = C_{D\text{ind}}(\hat{\boldsymbol{\delta}}_f) + \lambda g(\hat{\boldsymbol{\delta}}_f) \tag{32}$$

in which the constraint equation is

$$g(\hat{\boldsymbol{\delta}}_f) = C_L C_{Ba,1} + C_{Bb,0} + C_{Bb,1}\hat{\delta}_{f,1} + \cdots + C_{Bb,N}\hat{\delta}_{f,N} - C_{B\text{desired}} = 0 \tag{33}$$

The new system of equations to be solved for determining the optimum variation flap angles for minimizing induced drag with the bending moment constraint is written in matrix form as

$$\begin{bmatrix} C_{D11} & \cdots & C_{D1N} & C_{Bb1} \\ \vdots & & \vdots & \vdots \\ C_{DN1} & \cdots & C_{DNN} & C_{BbN} \\ W_1 & \cdots & W_N & 0 \\ C_{Bb1} & \cdots & C_{BbN} & 0 \end{bmatrix} \begin{Bmatrix} \hat{\delta}_{f,1} \\ \vdots \\ \hat{\delta}_{f,N} \\ \lambda/2 \end{Bmatrix} = -\begin{Bmatrix} C_L C_{Da1} + C_{D01} \\ \vdots \\ C_L C_{DaN} + C_{D0N} \\ 0 \\ C_L C_{Ba,1} + C_{Bb,0} - C_{B\text{desired}} \end{Bmatrix} \tag{34}$$

The solution of the overdetermined system of $(N + 2)$ equations yields the values of the N unknown variation flap angles and the Lagrange multiplier, λ.

IV. Results

Three examples are presented in this section to demonstrate the current approach. The examples have been chosen to illustrate the capabilities of the method rather than to recommend specific adaptive-wing configurations for use on aircraft.

In the first two examples, a planar wing of aspect ratio 12 for a hypothetical general aviation aircraft is used. The wing is assumed to have five TE flaps, all of equal span and a flap-to-chord ratio of 0.2. The WINGS discrete-vortex Weissinger method code has been used to compute the **D** matrix and associated information for these examples. The first example focuses on drag reduction at multiple values of aircraft C_L. Postdesign analysis using the WINGS code and aircraft-performance simulations are used to verify the results from the current approach. The second example illustrates the use of TE flaps for limiting the wing root bending moment.

The third example uses a nonplanar wing, with a 90 deg winglet of height $0.1b/2$ added to the planar wing of aspect ratio 12. The planar portion has three flaps with different spans and different flap-to-chord ratios, and the winglet also has a TE flap. This example is used to demonstrate the use of the current approach to nonplanar wings and wings with TE flaps of different sizes. The AVL code [24] has been used to determine the **D** matrix and associated information and for postdesign analysis.

A. Example 1: Drag Reduction on Planar Wing

For this example, a planar wing of aspect ratio 12 for a hypothetical general aviation aircraft is used. Table 1 lists the overall specifications of the hypothetical aircraft.

Figure 4 shows the wing–tail geometry used for the hypothetical aircraft. For the adaptive wing, five TE flaps have been used along the half-span, each with equal span and a flap-to-chord ratio of 0.2. The tail has been used for trimming the aircraft about the center of gravity, which is located to result in a stick-fixed static margin of 10% of the wing mean aerodynamic chord. A single NLF airfoil, custom designed for this wing, has been used along the span, and the wing twist is assumed to be zero.

For the postdesign performance comparisons that follow, the aircraft C_D was calculated at several values of aircraft C_L by adding the contributions of wing profile C_D, the trimmed-aircraft $C_{D\text{ind}}$, and a constant value of parasite C_D due to fuselage and other parts of the aircraft. The wing profile C_D was determined by integrating the contributions of the airfoil C_d for all the sections of the wing, each obtained from an airfoil drag polar, predicted using the XFOIL code [25] for the appropriate Reynolds number and flap setting. The $C_{D\text{ind}}$ was computed using the WINGS code for the trimmed configuration with the appropriate flap settings for the wing flaps. In the analysis of the configuration using the WINGS code, the section pitching moments (including flap contributions) were computed using section C_m information from XFOIL-predicted polars. The horizontal-tail

Table 1 Assumed geometry, drag, and power characteristics for the hypothetical general aviation airplane for Example 1

Parameter	Value
Gross Weight	14,200 N (3200 lbf)
Wing reference area	12.0 m^2 (130 ft^2.)
Wing aspect ratio	12
Equivalent parasite drag area of airplane minus wing	0.13 m^2 (1.4 ft^2.)
Rated engine power	200 kW (268 hp)
Propeller efficiency	85%, constant
Specific fuel consumption	8.31×10^{-7} N/s/W (0.5 lbf/h/hp)
Fuel volume	300 l (80 U.S. gal)

incidence was automatically adjusted to trim the aircraft about the c.g., thus taking into account the effects of flap pitching moments on the trim drag. The C_D contribution from interference, fuselage, and other parts of the aircraft was determined using the assumed value of the equivalent parasite drag area of the airplane minus wing, $C_{Df}S_f$, listed in Table 1. The aircraft C_D, which includes C_D due to trim, was then used to determine the power required for the corresponding flight velocity using standard techniques.

Figure 5a shows the airfoil geometry and Fig. 5b shows the drag polar for the airfoil at $Re\sqrt{C_l} = 3 \times 10^6$, as computed using the XFOIL code [25]. This value of $Re\sqrt{C_l}$ corresponds to rectilinear flight at standard sea-level conditions. It is seen that the low-drag range for the unflapped airfoil extends from $C_l = 0.33$ to 0.75. Using the information in this polar and the airfoil–aircraft integration approach described in [26], the ideal C_L for the level-flight maximum speed for the aircraft was determined to be approximately 0.15 and the ideal C_L for the maximum range was determined to be 0.73. Based on these estimates, it was decided that the wing would need to be adapted for low drag over a range of lift coefficients from 0.1 to 0.9. From the XFOIL-predicted drag polars for the wing airfoil, the $\delta_{f_{\min}}$ and $\delta_{f_{\max}}$ were chosen to be −10 and +10 deg, respectively, resulting in $C_{l\text{low}}$ of 0.1 and $C_{l\text{up}}$ of 0.9. This information was used along with Eq. (26) in determining the $\bar{\delta}_f$ for this wing.

Figure 6 shows the spanwise C_l distributions from the WINGS code for three values of the design C_L: 0.1, 0.5, and 0.9. In each case, the flaps were set to the optimum angles, as determined by the current approach. Superposed on each of the spanwise-C_l plots are the drag polars (sections C_d–C_l plots) for each portion of the wing from the XFOIL analysis, with the five C_d scales on top of the plot. The flap angles for each portion of the wing are also listed in the plot. The results demonstrate that the optimum flap-angle distributions ensure that each section C_l corresponds to a point within the appropriate drag bucket. Also to be noted is that the angle for any given flap varies smoothly with the flight condition. To put this result in perspective, Fig. 7 shows the C_l distributions for the three wing C_L values for the nonadapted wing with all flaps set to 0 deg, and the corresponding section drag polars for $\delta_f = 0$ deg. It is seen for

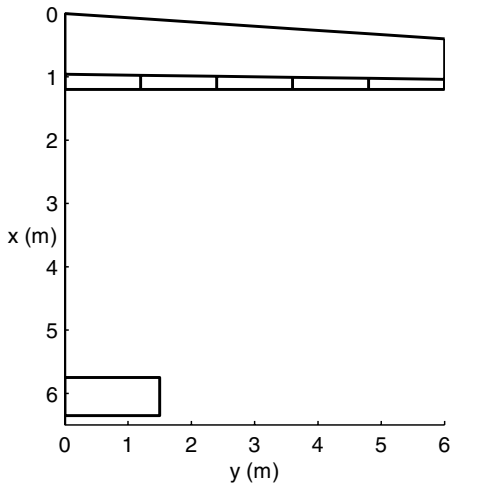

Fig. 4 Wing and tail geometry for example 1.

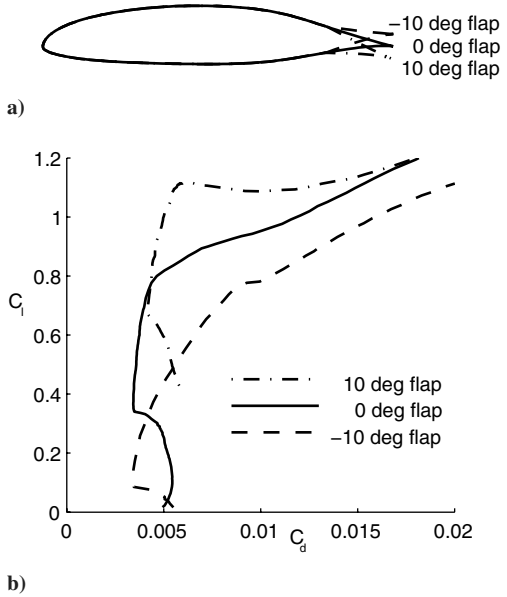

Fig. 5 NLF airfoil used for the wing: a) geometry, and b) drag polars from XFOIL analysis for $Re\sqrt{C_l} = 3 \times 10^6$.

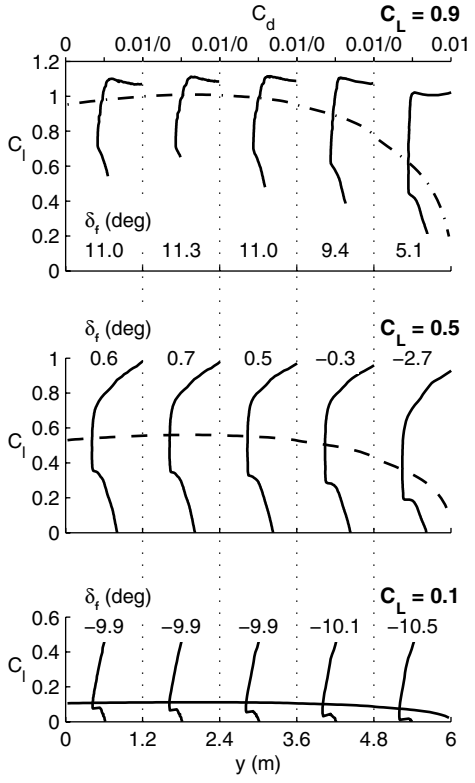

Fig. 6 Spanwise C_l distributions and drag polars for the adapted wing for $C_L = 0.9$, 0.5, and 0.1.

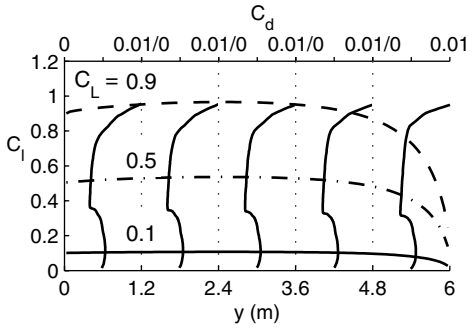

Fig. 7 Spanwise C_l distributions and drag polars for the nonadapted wing (all flaps set to 0 deg).

$C_L = 0.1$ and 0.9, the section C_l values for most of the wing do not lie within the low-drag range, indicating that these portions of the wing do not have extensive laminar flow.

Figure 8 shows the spanwise nondimensional lift distributions (cC_l/c_{average}) for these three values of C_L for the adapted wing with optimum flap angles as well as for the nonadapted wing with all flaps set to 0 deg. The minimum-induced-drag elliptical lift distributions, shown for reference, reinforce the fact that the lift distributions for the adapted case for each C_L closely match the desired elliptical loading.

To determine if the predicted flap-angle distributions are indeed the best for each C_L, postdesign analysis and aircraft-performance prediction were used. For this purpose, the wing with the flap schedules was analyzed using the WINGS code at the three values of C_L. In these analyses, the contributions due to both the trimmed-aircraft induced and profile drag were included. Figure 9 presents the total wing C_D as a function of wing C_L for four cases: 1) all flaps set to zero, 2) flaps set for $C_L = 0.1$, 3) flaps set for $C_L = 0.5$, and 4) flaps set for $C_L = 0.9$. It is clearly seen that the optimum flap schedule for a given C_L, as determined by the current approach, results in the least drag at that C_L. This result demonstrates the effectiveness of the current approach in determining the optimum flap angles for a given C_L.

To examine the performance benefits due to the different flap-angle variations, the drag predictions from WINGS were used in PERF, an aircraft-performance code [26]. Figures 10a–10c show comparisons of the aircraft rate of climb, range, and endurance as a function of airspeed at standard sea-level conditions. The results show that 1) for the case with the flaps optimized for $C_L = 0.1$, the $V_{\max}$ is significantly greater than those for the other cases by around 10 mph, and 2) the case with the flaps optimized for $C_L = 0.9$ results in the maximum range and the maximum endurance, with the maximum endurance a 9% improvement when compared with the case with all flaps set to zero. This performance comparison clearly illustrates the benefits of the use of multiple TE flaps for drag reduction and performance improvement.

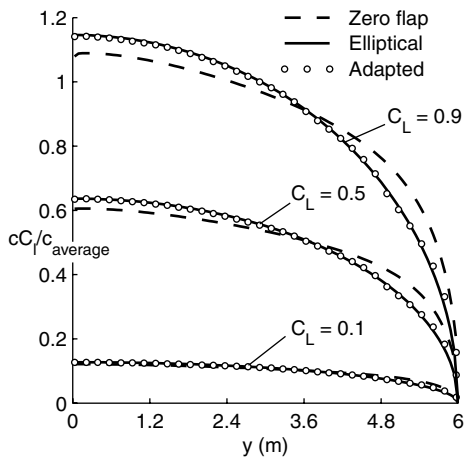

Fig. 8 Spanwise lift distributions for $C_L = 0.1$, 0.5, and 0.9 for the adapted and nonadapted wings compared with elliptical loading.

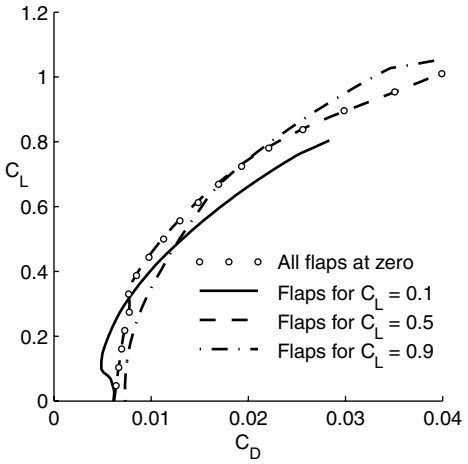

Fig. 9 Wing drag polars for zero flaps and for flaps optimized for $C_L = 0.1$, 0.5, and 0.9.

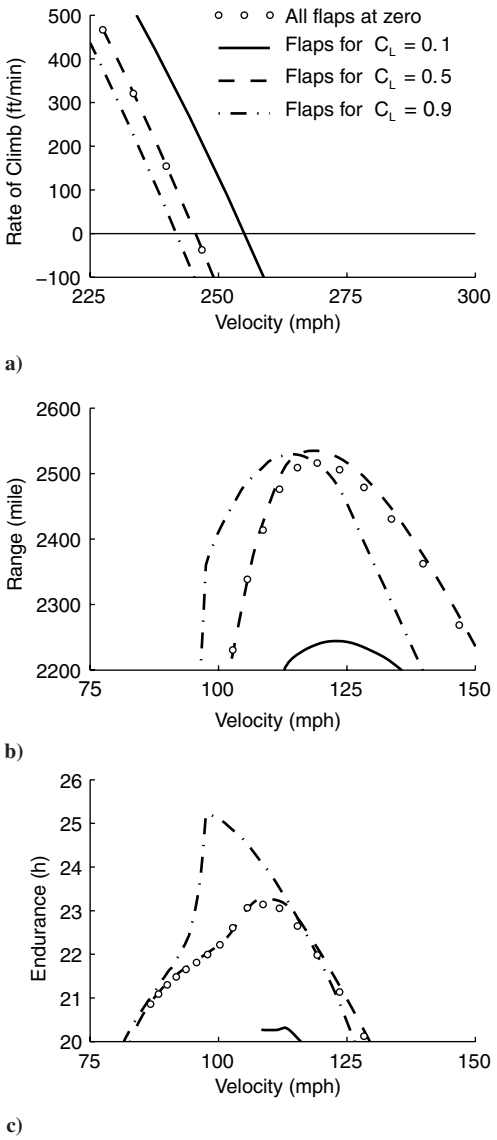

Fig. 10 Examination of performance benefits: a) rate of climb, b) range, and c) endurance.

B. Example 2: Bending Moment Alleviation on Planar Wing

In the next part of the study with this example wing, the use of multiple TE flaps for root bending moment alleviation at high load

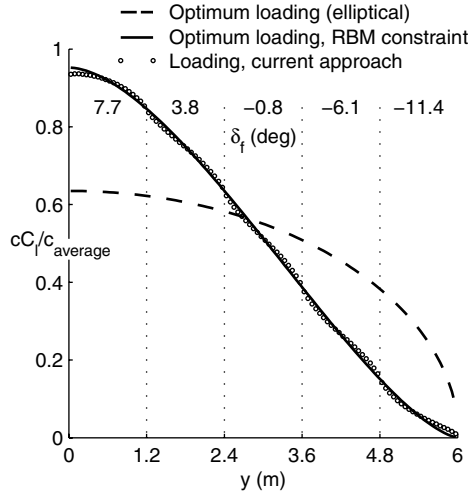

Fig. 11 Spanwise loading for $C_L = 0.5$ resulting from flaps set for root bending moment alleviation compared with the optimal loading from the method of Jones [27].

factors was explored. For this case, it was assumed that the aircraft is flying at a load factor of 4 g, but the design root bending moment corresponds to that experienced by the wing at 3 g when elliptically loaded. Therefore, the RBM constraint was prescribed to be 75% of the root bending moment for elliptical loading. The design C_L was chosen to be 0.5. Figure 11 shows the spanwise lift distribution from the WINGS code using the flap angles predicted by the approach. The flap angles are also listed in Fig. 11. Also shown for comparison are 1) the lift distributions for minimum induced drag with the RBM constraint from the analytical method of Jones [27], and 2) the elliptical loading for minimum induced drag without any constraint. It is seen that the loading from the current approach closely matches the optimum loading from the method of Jones.

It is to be noted that, for high C_L and larger root bending moment alleviations, the flap angles could be fairly large and could result in flow separation off the flap, leading to reduced flap effectiveness. This reduced effectiveness has not been taken into consideration in the current analysis. Additionally, the rigid wing assumption may also not be correct, particularly at high dynamic pressures. These two factors need to be taken into consideration in a more refined version of the current approach. Nevertheless, the results demonstrate that the approach is successful in predicting the required flap-angle variation. The results also provide confidence that the multiple TE flaps are successful in relieving the root bending moment and can thus be used to design wings of lower weight.

C. Example 3: Nonplanar Wing

The third example uses the same wing planform from the previous examples for the planar portion and has a 90 deg winglet of height $0.1b/2$ added to the wing tip. The planar portion has three flaps with different spanwise extents and different flap-to-chord ratios. The winglet also has a 15% chord TE flap. There is a small transition segment on the bottom of the winglet that is used to join the wing tip with the root of the winglet. This transition segment is unflapped. Figure 12 shows the geometry. This example is used to illustrate the application of the approach to a wing that has unequal flap sizes and has nonplanar geometry. The planar portion has the same airfoil as that shown in Fig. 5; the winglet has an airfoil designed for lower Reynolds numbers.

The optimum flap angles were determined by the current approach for a wing C_L of 0.1 and 0.9. Figures 13a and 13b show the resulting C_l distributions. Superposed on each plot are the XFOIL-predicted drag polars for each portion of the wing, with the C_d scales shown on top of the plot. The C_l distributions corresponding to the loadings for minimum induced drag from Munk's theory [15] are also shown for reference. It can be seen that the optimum flap angles for these flight conditions not only ensure that most section C_l values correspond to

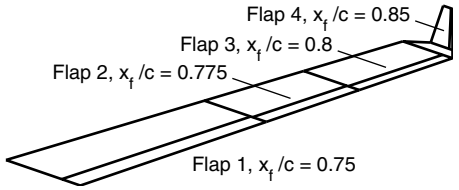

Fig. 12 Geometry of nonplanar wing.

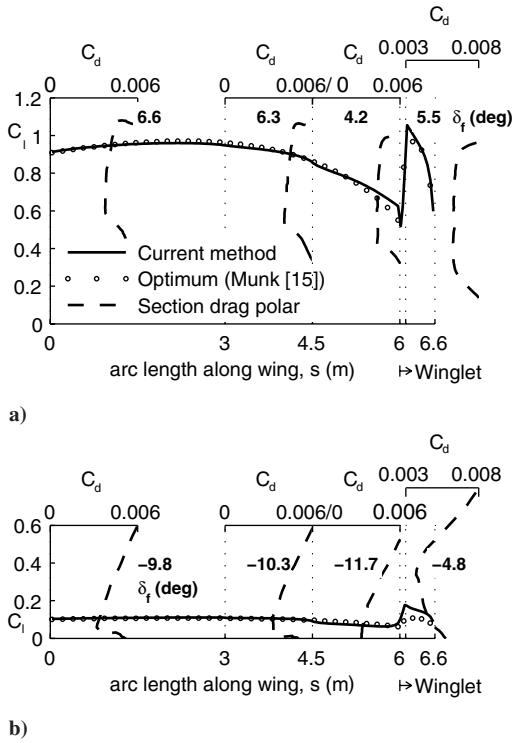

Fig. 13 Spanwise C_l distributions and drag polars for the nonplanar wing: a) flaps optimized for $C_L = 0.9$, and b) flaps optimized for $C_L = 0.1$.

points inside the respective drag buckets but also produce a loading that closely matches the optimum distribution for minimum induced drag.

The addition of the winglet significantly increases the design complexity for this example because of the need to consider the effects of the winglet airfoil, incidence, and chord distribution on the induced and profile drag. These effects are discussed in greater detail in [28]. When the 90 deg winglet, as used in this example, is equipped with a TE flap, this flap angle gets altered only for induced-drag minimization through the variation flap-angle distribution. Changes to the mean flap have no effect on the TE flap of a 90 deg winglet. Thus, the winglet flap angles suggested by the current approach are selected by the method for the minimization of induced-drag only. For some geometries, it may be desirable for the designer to use a different set of flap angles for the winglet as it may be more beneficial to enable operation of the winglet within the section drag bucket, even at the cost of off-optimal loading on the winglet. Alternatively, if the winglet TE flap, set for induced-drag minimization, is also intended to allow the winglet to operate within the section drag bucket, then, for a given winglet height, the average winglet chord, the winglet airfoil, and winglet incidence all need to be appropriately selected. In general, the use of a TE flap on the winglet may allow for a smaller winglet chord (for a given height) while enabling the same level of induced-drag reduction and allowing for the operation of the winglet within the drag bucket. As a result of the reduced wetted area, the profile drag can be decreased in comparison with a winglet without a TE flap.

V. Conclusions

With increasing interest in the use of multiple trailing-edge flaps for future adaptive wings, the objective of the current work was to provide an approach for determining the optimum flap angles at various flight conditions. An important element of the approach was the decomposition of the flap-angle distribution into 1) a mean flap that allows operation of the wing sections within the low-drag ranges for minimizing profile drag, and 2) a variation flap-angle distribution that can be used to minimize induced drag with or without a wing root bending moment constraint. The methodology uses superposition of basic and additional load distributions to linearize the problem, which enables a simple solution procedure that also provides insight. The methodology can also be adapted for other wing-design problems, such as determining optimum twist distributions and tailoring wing sections to ensure operation within the drag bucket.

In the current study, the optimum flap-angle distributions for different flight conditions were determined for two example wings. Using postdesign analysis, it is shown that both induced and profile drag were minimized over a wide range of wing lift coefficients using the optimum flap-angle distributions. The performance benefits due to the optimum flap angles were also computed for the trimmed airplane, with an observed increase in maximum velocity, maximum range, and maximum endurance when compared with the zero-flap setting case. The trailing-edge flaps were also found to be successful in relieving the root bending moment when using the optimized flap angles determined by the current approach with the prescribed root bending moment constraint. Thus, the current approach is seen to be effective in determining trailing-edge flap angles for either a reduction in drag or a reduction in drag with a bending moment constraint.

In addition to drag reduction, the use of multiple trailing-edge flaps provides the opportunity for redundant control effectors for roll control, as well as a reduction in structural wing weight through active load control. However, for these benefits to be realized, there is a need to further develop flap-actuation technology for rapid and reliable actuation of the flaps at the onset of high load factors during maneuvering and for flight in gusty conditions. Overall, the decision on whether to use multiple flaps for a particular aircraft concept will depend on system-level considerations, such as whether the benefits of multiple trailing-edge flaps outweigh the penalties in weight and complexity. With continuing improvements in actuator and control-system technologies and increasing pressures to reduce fuel burn, it is likely that multiple flaps will play an important role on future aircraft.

Acknowledgments

This research was funded by NASA Langley Research Center contract NNL04AA33C. Helpful discussions with technical monitors Jeffrey Flamm and William Milholen are acknowledged. Helpful discussions with Mark Maughmer on winglet design are also acknowledged. Partial support for the second author was also provided by the Frank C. Ziglar, Jr., Endowed Graduate Fellowship and is acknowledged.

References

[1] Spillman, J. J., "The Use of Variable Camber to Reduce Drag, Weight and Costs of Transport Aircraft," *The Aeronautical Journal*, Vol. 96, No. 951, Jan. 1992, pp. 1–9.

[2] Thornton, S. V., "Reduction of Structural Loads Using Maneuver Load Control in the Advanced Fighter Technology Integration (AFTI)/F-111 Mission Adaptive Wing," NASA TM 4526, Sept. 1993.

[3] Wlezien, R. W., Horner, G. C., McGowan, A. R., Padula, S. L., Scott, M. A., Silcox, R. J., and Simpson, J. O., "The Aircraft Morphing Program," AIAA Paper 98-1927, April 1998.

[4] Bolonkin, A., and Gilyard, G. B., "Estimated Benefits of Variable-Geometry Wing Camber Control for Transport Aircraft," NASA TM 1999-206586, Oct. 1999.

[5] Stanewsky, E., "Aerodynamic Benefits of Adaptive Wing Technology," *Aerospace Science and Technology*, Vol. 4, No. 7, 2000, pp. 439–452.
doi:10.1016/S1270-9638(00)01069-5

[6] Monner, H. P., Breitbach, E., Bein, T., and Hanselka, H., "Design Aspects of the Adaptive Wing—The Elastic Trailing Edge and the Local Spoiler Bump," *The Aeronautical Journal*, Vol. 104, No. 1032, Feb. 2000, pp. 89–95.

[7] Phillips, W. F., Alley, N. R., and Goodrich, W. D., "Lifting-Line Analysis of Roll Control and Variable Twist," *Journal of Aircraft*, Vol. 41, No. 5, Sept.–Oct. 2004, pp. 1169–1176.
doi:10.2514/1.3846

[8] Fielding, J. P., "Design Investigation of Variable-Camber Flaps for High-Subsonic Airliners," *Proceedings of 2000 International Council of the Aeronautical Sciences*, International Council of the Aeronautical Sciences, Stockholm, Sweden, 2000, pp. 124.1–124.11.

[9] Reich, G. W., Bowman, J. C., and Sanders, B., "Large-Area Aerodynamic Control for High-Altitude Long-Endurance Sensor Platforms," *Journal of Aircraft*, Vol. 42, No. 1, Jan.–Feb. 2005, pp. 237–244.
doi:10.2514/1.7146

[10] Anderson, R. F., "Determination of the Characteristics of Tapered Wings," NACA Rept. 572, 1936.

[11] Abbott, I. H., and von Doenhoff, A. E., *Theory of Wing Sections*, McGraw–Hill, New York, 1949.

[12] Kuethe, A. M., and Chow, C.-Y., *Foundations of Aerodynamics: Bases of Aerodynamic Design*, Wiley, New York, 1986.

[13] Robinson, A., and Laurmann, J. A., *Wing Theory*, Cambridge Aerospace Series, Cambridge Univ. Press, Cambridge, England, UK, 1956.

[14] Katz, J., and Plotkin, A., *Low-Speed Aerodynamics*, Cambridge Aerospace Series, 2nd ed., Cambridge Univ. Press, Cambridge, England, UK, 2001.

[15] Munk, M. M., "The Minimum Induced Drag of Aerofoils," NACA Rept. 121, 1921.

[16] Bryson, A. E., Jr., and Ho, Y.-C., *Applied Optimal Control*, Wiley, New York, 1975.

[17] Pfenninger, W., "Investigation on Reductions of Friction on Wings, in Particular by Means of Boundary Layer Suction," NACA TM 1181, Aug. 1947.

[18] Pfenninger, W., "Experiments on a Laminar Suction Airfoil of 17 Per Cent Thickness," *Journal of the Aeronautical Sciences*, Vol. 16, No. 4, April 1949, pp. 227–236.

[19] Somers, D. M., "Design and Experimental Results for a Flapped Natural-Laminar-Flow Airfoil for General Aviation Applications," NASA TP 1865, June 1981.

[20] McGhee, R. J., Viken, J. K., Pfenninger, W., Beasley, W. D., and Harvey, W. D., "Experimental Results for a Flapped Natural-Laminar-Flow Airfoil with High Lift/Drag Ratio," NASA TM 85788, May 1984.

[21] Althaus, D., and Wortmann, F. X., *Stuttgarter Profilkatalog I*, Friedr. Vieweg & Sohn Verlagsgesellschaft, mbH, Braunschweig/Wiesbaden, Germany, 1981.

[22] Drela, M., "Elements of Airfoil Design Methodology," *Applied Computational Aerodynamics*, edited by P. A. Henne, Vol. 125, AIAA, Washington, DC, 1990, pp. 167–189.

[23] Althaus, D., *Niedriggeschwindigkeitsprofile*, Friedr. Vieweg & Sohn Verlagsgesellschaft, mbH, Braunschweig/Wiesbaden, Germany, 1996.

[24] Drela, M., and Youngren, H., *AVL 3.26 User Primer*, Department of Aeronautics and Astronautics, Massachusetts Institute of Technology, Cambridge, MA, 2006.

[25] Drela, M., "XFOIL: An Analysis and Design System for Low Reynolds Number Airfoils," *Low Reynolds Number Aerodynamics*, edited by T. J. Mueller, Vol. 54, Lecture Notes in Engineering, Springer–Verlag, New York, June 1989, pp. 1–12.

[26] Gopalarathnam, A., and McAvoy, C. W., "Effect of Airfoil Characteristics on Aircraft Performance," *Journal of Aircraft*, Vol. 39, No. 3, May–June 2002, pp. 427–433.
doi:10.2514/2.2968

[27] Jones, R. T., "The Spanwise Distribution of Lift for Minimum Induced Drag of Wings Having a Given Lift and a Given Bending Moment," NACA TN 2249, Dec. 1950.

[28] Maughmer, M. D., "Design of Winglets for High-Performance Sailplanes," *Journal of Aircraft*, Vol. 40, No. 6, Nov.–Dec. 2003, pp. 1099–1106.
doi:10.2514/2.7220